

Lithium-Phase Identification in an Industrial Lithium-Ion-Battery Recycling Slag: Implications for the Recovery of Lithium

Peter Cornelius Gantz,* Louisa Panjiyar, Andreas Neumann, Michael Neumann, Hans Roggendorf, Ralf Wehrspohn, Stefan Stöber, and Christiane Stephan-Scherb*

The recycling of lithium-ion batteries (LIBs) through extractive pyrometallurgy is widely used, but a significant drawback is the loss of lithium to the slag. To address this, lithium-bearing slag from an industrial LIB recycling plant is analyzed using wavelength dispersive X-ray fluorescence, inductively coupled plasma optical emission spectroscopy, X-ray diffraction (XRD), and thermogravimetry coupled infrared. The slag's chemical composition is complex, best described by the ternary system $\text{CaO-SiO}_2\text{-Al}_2\text{O}_3$, with additional major components being Na_2O , Fe_2O_3 , MgO , V_2O_5 , Mn_2O_3 , and Cr_2O_3 . The slag cone shows little chemical zonation and a relatively constant lithium content of \varnothing 0.82 mass%. The recycling slag shows a mineralogical composition typical of nonferrous slags (e.g., melilite, clinopyroxene, nepheline). Lithium is either bound in β -eucryptite or, to a lesser extent, in lithium metasilicate. β -eucryptite contains up to 5.51 mass% lithium stoichiometrically, which is more than typical lithium ores contain. Moreover, β -eucryptite has potential for the engineering of artificial minerals strategy as an easily implementable lithium phase. β -eucryptite forms in slags with lower overall lithium content, allowing for the use of slag modifiers that reduce the process temperature. Hence, β -eucryptite could prove as efficient and feasible option for improving lithium recovery from smelting processes.

required resources, with two options to obtain the required metals (Li, Cu, Co, Ni, Al):^[3] 1) the primary production of metals and minerals from mining to meet growing demand and 2) secondary production from recycling to protect and conserve natural resources.^[3,4]


The new EU battery directive puts a strong emphasis on the recycling of LIBs by introducing specific recycling quotas.^[5] From 2027, 50% of the lithium contained in LIBs must be recovered.^[5] Quotas have also been introduced for the use of recycled lithium in new LIBs.^[5] In 2031, 6% of the lithium used in new LIBs must be recycled lithium, and by 2036, the minimum required recycled lithium content in newly manufactured LIBs will double to 12%.^[5] To comply with this regulation, a lithium recovery rate of at least 80% must be achieved by 2031, assuming a collection rate of 100% for spent LIB.^[6,7] Currently, recycling of most battery metals (Cu, Co, Ni) is already established using extractive pyrometallurgy.^[8]

One major issue is the accumulation of lithium in the slag, resulting in significant dilution due to added slag formers and slag modifiers. Furthermore, the slag is frequently enriched with potentially environmentally hazardous heavy metals, e.g., Cu, Ni, and Pb.^[9,10] The mineral phases finally contain the lithium depend on different factors, i.e., composition of the slag, maximum process temperature, or the cooling rates.^[11] To date, the lithium from such slags is not extracted

1. Introduction

Lithium-ion batteries (LIBs) are part of everyday life, as they are widely used in portable electronic devices, and there will be an increasing demand in the road transport sector as part of electric vehicles (EV),^[1] with the demand only rising in the foreseeable future.^[2] There is a discussion about the future supply of the

P. C. Gantz, L. Panjiyar, A. Neumann, S. Stöber, C. Stephan-Scherb
Institute for Geosciences and Geography
Martin-Luther-University Halle-Wittenberg
06120 Halle (Saale), Germany
E-mail: peter.gantz@student.uni-halle.de;
christiane.stephan-scherb@geo.uni-halle.de

 The ORCID identification number(s) for the author(s) of this article can be found under <https://doi.org/10.1002/aesr.202400338>.

© 2024 The Author(s). Advanced Energy and Sustainability Research published by Wiley-VCH GmbH. This is an open access article under the terms of the Creative Commons Attribution License, which permits use, distribution and reproduction in any medium, provided the original work is properly cited.

DOI: 10.1002/aesr.202400338

P. C. Gantz, L. Panjiyar, A. Neumann, H. Roggendorf, R. Wehrspohn, S. Stöber
Center for Resources and Recycling (CRR)
ITEL – Institute for Technologies and Economics of Lithium GmbH
06108 Halle (Saale), Germany

M. Neumann
Nickelhütte Aue GmbH
08280 Aue, Germany

H. Roggendorf, R. Wehrspohn
Institute for Physics
Martin-Luther-University Halle-Wittenberg
06120 Halle (Saale), Germany

and the resulting slag is either landfilled or downcycled for the use as a building material.^[12] Either way, the lithium cannot be used to produce new batteries.

Regarding the challenging time schedule set by the EU, it is advisable to focus on a lithium extraction process using the already established extractive pyrometallurgical recycling as basis. One novel pyrometallurgical approach is the accumulation of a target element in a mineral phase. This “engineering of artificial minerals” (EnAM) approach is often discussed in recent literature as a strong option for lithium recovery.^[13–16]

To identify potential extraction processes for the lithium from the slag, a comprehensive understanding of the chemical boundary conditions of the lithium in products of extractive pyrometallurgical recycling is required. Therefore, this work focuses on the characterization of a lithium-bearing slag produced by smelting spent LIBs, using chemical and mineralogical analysis. This study aims to achieve a better understanding of how lithium is distributed in the recycling slag and in which mineral phases it is incorporated.

2. Pyrometallurgical LIB Recycling

2.1. Applied Processes

Pyrometallurgical processes can be subdivided into two categories: thermal pretreatment and extractive pyrometallurgy (Figure 1).^[17,18] The key distinctions between these processes are the employed temperature ranges and the resulting products.

Extractive pyrometallurgy requires higher temperatures; for instance, non-salt-assisted roasting usually begins at 650 °C and can reach up to 1200 °C.^[19,20] Smelting processes typically require temperatures exceeding 1250 °C^[21] and even up to 1700 °C.^[22] Depending on the exact process parameters, roasting produces a variety of different products, while smelting usually

produces the metals Ni, Co, and Cu as alloy or matte, in addition to a slag which contains the lithium (Figure 1).^[17,18]

Thermal pretreatment, including pyrolysis and incineration, operates over a wide range of temperatures, typically below 700 °C.^[18,23–25] Thermal pretreatment techniques aid in the production of black mass, an intermediate product of LIB recycling.^[18,25,26] Incineration should be conducted at a minimum temperature of 500 °C to break down the polyvinylidene fluoride binder.^[24] Pyrolysis provides the opportunity to break down the organic components and utilize them as fuel.^[27] Additionally, at low temperatures (<150 °C), it is possible to recover the electrolyte of the recycled LIBs through condensation.^[28]

2.2. The Slag Formation Process at Nickelhütte Aue

Smelting of LIBs, an extractive pyrometallurgical LIB recycling process, produces slags as a byproduct. In a batch process, complete batteries, other Ni- and Co-containing materials, and slag formers (i.e., sand, gypsum) are added into a rotary kiln. This mixture is heated up to 1350 °C by burning natural gas (Figure 2). At this temperature, the components melt completely.

Inside the furnace, two immiscible melts, one silicate melt ($A_xSi_yO_z$; A = Ca, Al, Mg, Na, Li, K, Fe, Mn, Cr, V,...) and one sulfide melt (M_xS_y ; M = Ni, Cu, Co,...) form. These two melts have different densities and thus separate into two liquid layers. The lower layer is formed by the sulfide melt while the silicate melt forms the upper layer. The melts are poured into a steel cone, which is connected to two steel overflow cones (Figure 2). The sulfide melt fills up most of the central cone. The silicate melt remains on top of the central cone and fills up the two additional cones. The filled cones cool down to ambient conditions within two days. The solidification features two steps. 1) Formation of an amorphous outer layer: when the melt mixture encounters the cold steel cone, it quenches and mostly

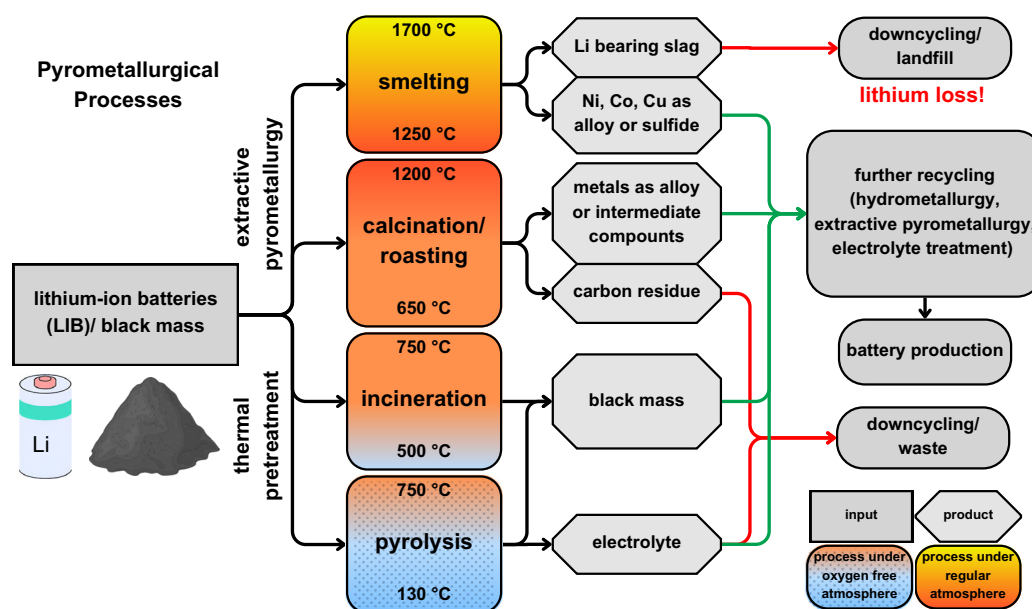


Figure 1. Visualization of the different pyrometallurgical recycling processes, showcasing input, processes with temperatures and atmospheric conditions, products, and further (processing) routes.

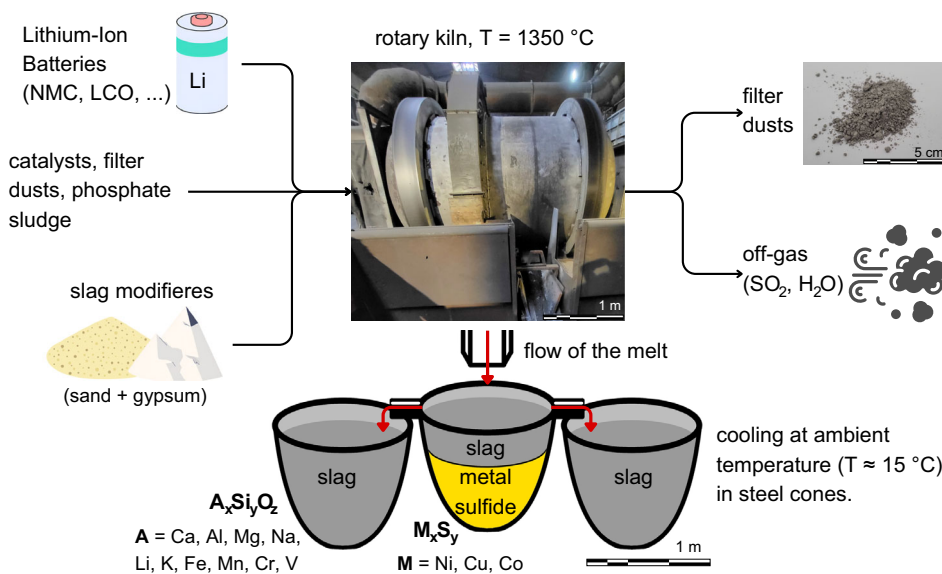


Figure 2. Schematic process of the LIB recycling process at Nickelhütte Aue.

an amorphous outer layer forms. This layer insulates the remaining melt from the temperature difference between the steel cone and the melt. 2) Crystallization of the mineral phases: the residual melt cools down more slowly, enabling the crystallization of mineral phases.

The central cone, i.e., the product cone contains solidified metal sulfides and a silicate slag cap on top. The two overflow cones, i.e., slag cones mainly contain silicate slag with minor amounts of metal sulfides. As the slag cones are positioned symmetrically around the product cone and cool down under the same conditions, no significant differences between the two slag cones are to be expected. The metal sulfides are the intermediate product of the recycling process. They are subjected to further refining, while the lithium-bearing slag is currently downcycled and used for roadworks or is landfilled.

3. Experimental Section

3.1. Sampling

Slags were sampled from the standard LIB-recycling process of Nickelhütte Aue GmbH. Samples were taken from the same batch as soon as the slag was cold enough for safe demolding and crushing. The slag was carefully broken using a jackhammer, mounted on an excavator. The product cone and one slag cone were sampled (Figure 3). The applied sampling scheme considered possible zonation within the cone. One cone has a diameter of 1 m at the top (Figure S1, Supporting Information).

3.2. Sample Description

All samples of the slag and product cone consisted mainly of crystalline solids of varying gray color (Figure S2, S3, Supporting Information). The peripheral part of the slag cone, represented by samples 1, 4, and 5, exhibited a mostly

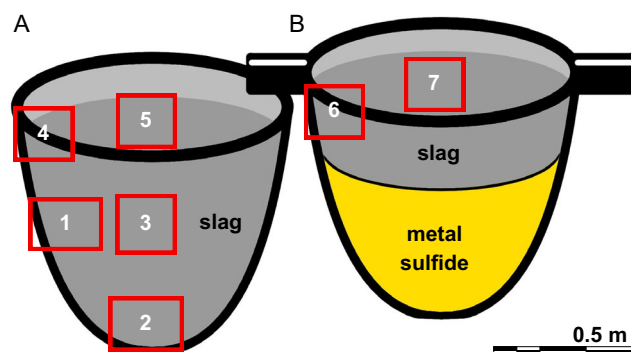


Figure 3. Schematic image of the product cone and one slag cone. The red rectangles show the approximate sampling positions. A) The slag cone and B) the product cone.

amorphous layer which has a maximum thickness of ≈ 2 cm. Visible mineral crystals could be observed in the inner part of samples 1 and 2 and also in the center of slag cone (sample 3). In sample 1, an increase in crystal size from micrometer to millimeter scale from the outer to the inner part was apparent (Figure S2, Supporting Information). Sample 3 featured crystals and angular cavities larger than 1 cm (Figure S2, Supporting Information). All samples were mostly magnetic and feature small, rounded holes (with a maximum diameter of 2 mm). The slag layer of the product cone (sample no. 6 and 7) displayed a more distinct magnetism. Furthermore, a yellow to brown discoloring was visible, which was not occurring in the slag cone. These samples contained increased amounts of rounded cavities of up to 1 cm in size (Figure S3, Supporting Information).

3.3. Sample Preparation

Representative parts of the samples were crushed using a jaw crusher and milled for 1–3 min at 700–1400 rpm using the

Retsch RS 1 vibratory disk mill, to obtain fine powder for X-ray diffraction (XRD) and wavelength dispersive X-ray fluorescence (WDXRF) analyses. For samples 1 and 5, additional subsamples were taken from the mostly amorphous outer layer of the cooled and hardened slag (samples 1a and 5a).

3.4. Methods

The main goal of this study was to identify the Li-bearing phases and to understand the complex phase assemblage of the slag. Both are important information to develop recycling procedures for this material. For chemical analysis, quantitative as well as semiquantitative bulk analysis were performed by WDXRF, and the lithium content was measured by inductively coupled plasma optical emission spectroscopy (ICP–OES). The results of both methods could be evaluated and compared to check for a chemical zonation of the major and minor elements, or even the targeted lithium. Mineralogical characterization was performed by XRD.

3.4.1. ICP–OES and Quantitative Sulfur Measurements

For the lithium measurements with ICP–OES, the sample was dissolved into an aqueous solution and measured in accordance to DIN EN ISO 11885:2009-09.^[29] The material was prepared for acid digestion by performing alkaline fusion with Na₂O₂. The fused mixture was digested in aqua regia and diluted with deionized water for the ICP–OES measurements. For the quantitative sulfur measurements, the sample was burned in an induction furnace in an O₂ atmosphere to oxidize the sulfur to SO₂, which was detected by infrared spectroscopy (in accordance with DIN 51085:2015-01).^[30]

3.4.2. Wavelength-Dispersive X-Ray Fluorescence

WDXRF was used for the determination of the main and trace element composition. The gain on ignition (GOI) was determined by heating and holding 1 g of sample to 1000 °C for 1 h. This was performed twice per sample. Afterward, fused beads were prepared. An amount of 1 g of sample was mixed with 8 g of flux (LiB₄O₇, Supelco). Samples 1–5 were prepared as fused beads using the “Fusion Machine” (HD Elektronik und Elektrotechnik GmbH).

Samples 6 and 7 were prepared as pressed pellets, due to issues with the preparation using the flux method. For preparing pressed pellets, 8 g of finely ground sample was mixed extensively with 2 g of wax (Hoechst–Wachs) in an agate mortar. Fused beads are the standard for quantitative measurements to avoid potential error sources like uneven mixing and granulometric effects, which are present in pressed pellets.^[31] All fused beads were measured quantitatively using the “S8 Tiger 2” WDXRF Spectrometer (Bruker AXS). The quantitative XRF measurements were carried out by using the “GEO-QUANT ADVANCED” program, which included a specific calibration for the selected elements. The pressed pellets were measured semiquantitatively using the “QUANT-EXPRESS” program, which included more elements than the quantitative measurement program.

3.4.3. Qualitative Phase Analysis by XRD

XRD analysis was applied to characterize the bulk mineralogical composition of the slag. The measurements were performed with a Panalytical X’pert³ Powder (Malvern Panalytical) diffractometer using a Bragg–Brentano geometry and Cu–K α radiation. The diffractometer configuration for the incident beam path consists of a 10 mm mask, 0.04 rad Soller slits, a fixed 1/8° divergence slit, and a fixed 1/4° anti-scatter slit. For the diffracted beam path, a 7.5 mm anti-scatter slit, 0.04 rad Soller slits, and a Ni K- β filter were used. The data was collected by PIXcel 1D detector and a step size of 0.013°2 θ . The samples were prepared using flat sample holders and the back-loading method. And, 10% of silicon was added as an internal standard to correct the sample height error.

4. Results and Discussion

4.1. Chemical Characterization

A central question of this investigation was to test whether the slag is chemically homogeneous or if it shows chemical zonation. The slag cone (sample no. 1–5) contains a rather constant lithium concentration, as determined by ICP–OES (Table 1), ranging between 0.77 mass% Li in sample 4 and 0.9 mass% Li in sample 5a. The mean and median lithium concentration is 0.82 mass% Li. The standard statistical tool to compare the variability between populations of different scales is the coefficient of variation (CV).^[32] The CV is calculated by normalizing the standard deviation (σ) with the mean (μ) of the same population. The equation for calculating the CV is given in Equation (1). To give the CV in %, the result is to be multiplied by 100.

$$CV = \frac{\sigma}{\mu} \quad (1)$$

The CV for lithium in the slag cone is 4.9%, showing little variation; however, no spatial accumulation can be found. The quantitative sulfur content (Table 1), as determined by thermogravimetric analysis coupled with infrared (IR) spectroscopy, in the slag cone (sample no. 1–5) shows an overall low sulfur content with a mean of 0.32 mass% S but a high level of variation as shown by the CV of 46.52%. There are two reasons for the high variation of sulfur in the slag cone: 1) the samples from the top of the slag cone (sample no. 5a and 5b) show an increased sulfur

Table 1. Quantitative results for the lithium and sulfur content (mass%) as well as gain on ignition (GOI) of all seven samples, as determined by ICP–OES and thermogravimetry-coupled IR spectroscopy, respectively.

Sample	Slag cone ^{a)}							Product cone	
	1a	1b	2	3	4	5a	5b	6	7
Li [mass%]	0.82	0.79	0.83	0.78	0.77	0.90	0.83	0.52	0.75
S [mass%]	0.30	0.21	0.20	0.27	0.20	0.64	0.39	9.72	2.58
GOI [%]	0.76	0.41	0.47	0.4	0.43	1.59	1.06	8.2	3.72

^{a)}1a and 5a represent the amorphous outer layer of the respective subsample, while 1b and 5b represent the mostly crystalline inner part of each sample.

level in comparison to the rest of the slag cone; 2) the amorphous subsamples (sample no. 1a and 5a) show an increased sulfur content compared to their crystalline (sample nos. 1b and 5b) counterparts, with 0.30 mass% S (sample 1a) to 0.21 mass% S (sample 1b) and 0.64 mass% S (sample 5a) to 0.39 mass% S (sample 5b), respectively.

The product cone (sample no. 6 and 7) contains less lithium than the slag cone (Table 1) with strongly varying total amounts. The sulfur levels also vary greatly (Table 1) but are increased compared to the slag cone. All samples display a negative loss on ignition, which translates to an increase in mass on ignition, referred to as GOI.^[33] The GOI of all samples is shown in Table 1. The GOI is likely caused by the oxidization of sulfide S^{2-} to sulfate $(SO_4)^{2-}$, e.g., the oxidation of the sulfide minerals at higher temperatures and the formation of sulfate phases with oxygen from the air (Equation (2)).^[34] This implies a linear correlation between sulfur content and GOI.^[34]



However, the GOI shows a nonlinear correlation to the quantitative sulfur content (Figure 4). There are two processes able to distort the correlation GOI and sulfur content: 1) incomplete oxidation of sulfide minerals in the samples with high sulfur content; 2) loss of volatile components during heating. Incomplete oxidation of the sulfides would decrease the GOI of the high sulfur samples, while the loss of volatile components would increase the GOI of low sulfur samples. Both processes lead to a similar distortion of the correlation of GOI and sulfur content. Additionally, an inverse correlation between lithium content on and sulfur content is apparent (Figure 4). Hence, lithium is proven to be not associated with the sulfide minerals.

The chemical composition, as determined by WDXRF, of the slag is rather complex with SiO_2 , CaO , and Al_2O_3 as main components only contributing around 75.3 ± 1.6 mass%. Further main components, i.e., >1 mass%, are Fe_2O_3 , Na_2O , MgO , V_2O_5 , Mn_2O_3 , and Cr_2O_3 (Figure 5). The minor components, i.e., <1 mass%, are ZnO , P_2O_5 , BaO , TiO_2 , NiO , K_2O , CuO , SrO , and ZrO_2 (Figure 6a). The CV for each component of

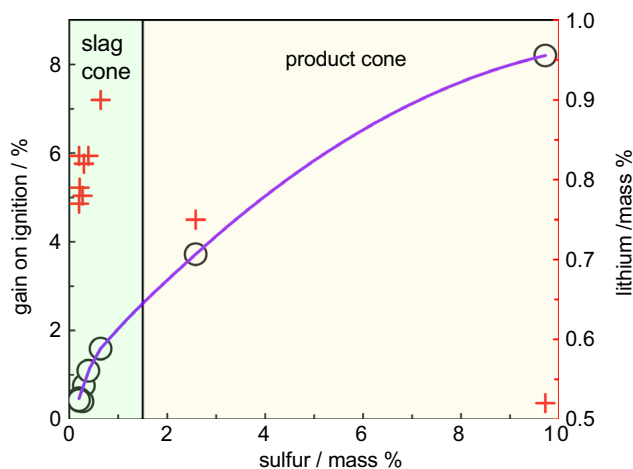


Figure 4. Sulfur content (mass%) of all samples plotted against the gain on ignition and lithium content (mass%). Purple line as guide to the eye.

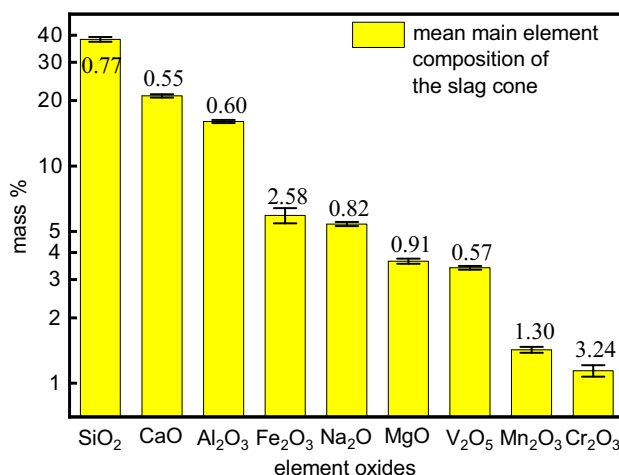


Figure 5. Mean quantitative major element composition, as determined by WDXRF, of the slag cone (sample no. 1a–5b) with coefficient of variation and extreme values.

the slag cone (sample no. 1–5) was calculated to assess the variation in composition. Due to the high SiO_2 and Al_2O_3 content, it is likely that the slag cone mostly consists of different silicate minerals or a complex silicate glass.

Furthermore, the displayed distribution of the main components is very homogenous. Most main compounds show very little deviation over the slag cone, with a CV below or close to 1%. This suggests that there is little elemental transport inside the solidifying slag cone. Therefore, a similar mineralogical composition over the entire slag cone is expected. The only exceptions are Fe and Cr showing a CV of 2.58% and 3.24%, respectively.

The higher CV of iron can be traced back to samples 5a, 5b, and 1a showing an increased iron content of 6.06 ± 0.15 mass% compared to the mean Fe_2O_3 content of the other samples of 5.93 ± 0.03 mass%. The samples with an increased iron content also contain more sulfur than the rest of the slag cone. Therefore, it is likely that some Fe is bound in the sulfides which show a highly uneven distribution. The Cr_2O_3 distribution in the slag cone is slightly uneven, with sample 5a showing the lowest Cr_2O_3 content with 1.06 ± 0.002 mass%, while sample 3 contains the highest Cr_2O_3 content with 1.17 ± 0.003 mass%. The Cr_2O_3 content does not correlate with the sulfur content and has a higher CV as the silicate phases. This makes it likely that the Cr_2O_3 is bound in a slightly unevenly distributed oxide phase. A likely candidate is a Cr_2O_3 -containing spinel (general formula: $A^{2+}B^{3+}_2O_4$ with A and B are 2+ and 3+ valent metals), forming a typical oxide slag mineral.^[35,36]

For the minor components, a polymodal distribution is apparent. ZnO , P_2O_5 , BaO , and TiO_2 show the lowest CVs (between 0.58% and 1.21%). It is likely that they are associated with the homogeneously distributed silicates. Due to the higher sulfur content of samples 5a and 5b, they are plotted separately and are not included in the calculations of the CV. Still, the CVs for the sulfur-associated metals (Figure 6b) Ni (22.76%) and Cu (24.26%) are very high which further illustrates the heterogeneous distribution of sulfur in the slag cone. An increase in Ni, Cu, and S content in the amorphous outer layers of the slag was observed. In the smelting process, gravimetric separation

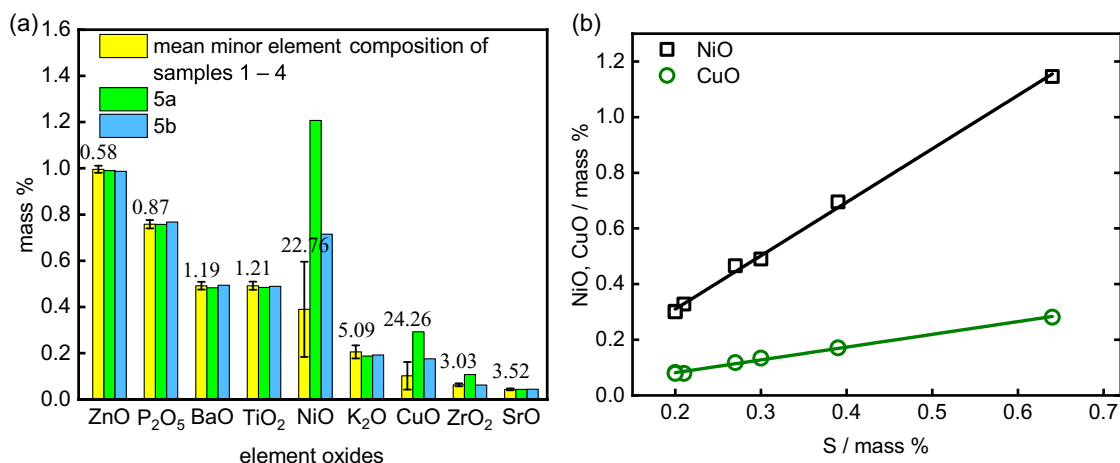


Figure 6. a) Mean quantitative minor element composition, as determined by WDXRF, of the slag cone. Sample 1a–4 with coefficient of variation and extreme values, subsamples 5a and 5b plotted separately. b) NiO and CuO plotted against S content, showing a linear correlation.

separates the metal sulfide from the slag. Hence, it is likely that gravimetric separation also takes place in the slag cone. Therefore, it is expected that the quickly cooled amorphous outer layers of the slag contain the average amount of Ni, Cu, and S of the slag cone. This implies that the main body of the slag cone is depleted in those elements and metal sulfides likely form a layer at the bottom of the slag cone.

K₂O, ZrO₂, and SrO have a CV of 5.09, 3.03, and 3.52%, respectively. However, for neither compound, a clear spatial trend could be recognized. The ZrO₂ and K₂O measurements have the two highest statistical errors with a mean of 2.18% and 0.70% respectively. The mean statistical error of the SrO measurement is 0.47%, which is average for this measurement. Consequently, the variation is likely due to sample preparation limitations in addition to the statistical error of the quantitative WDXRF measurements.

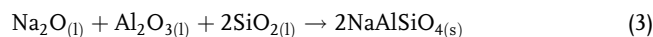
The concentration of the major components in the slag cap of the product cone (sample no. 6 and 7) could only be measured using a semiquantitative measurement program (Table 2), while the slag cone was measured quantitatively. Thus, care must be taken when comparing the absolute values. However, the sulfur concentration measured by quantitative thermogravimetric sulfur analysis and the semiquantitative WDXRF program are very close with 2.58 and 2.60 mass%, respectively. A noticeable difference in the chemical compositions of both cones can be detected. The major differences between both cones are the concentrations of sulfur and the associated metals (e.g., Ni, Cu). The samples from the product cone contain significantly more S, Ni, and Cu. A higher abundance of the metal sulfide phases indicates inversely a lower abundance of all others, mostly with associated silicate. Especially, the center of the slag cap (sample 6) exhibits

by far the highest sulfur levels. However, the rim of the slag cap (sample 7) shows a similar chemical composition to the samples from the slag cone.

4.2. Mineralogical Characterization

The mineral content of the slag was qualitatively analyzed by applying XRD and subsequent analysis of the diffraction patterns using HighScore Plus v 4.9.^[37] The results of the qualitative phase analysis are shown in Table 3. Pawley fitting, a structure independent fitting method for diffraction patterns,^[38] was performed using TOPAS 6.0.^[39] The Pawley fits are in good agreement with the qualitatively determined phases. Exemplary XRD patterns can be found in Supporting Information (Figure S4–S6, Supporting Information).

The only phases present in all samples are the silicates clinopyroxene and nepheline. An augite was selected for peak evaluation of the clinopyroxenes, but the true composition of the clinopyroxene in the slag could deviate to some extent, as clinopyroxenes are known for their variable chemical composition.^[40] Considering the presence of sodium together with aluminum in a silicate melt, the formation of nepheline in both cones is likely.^[41] Equation (3) demonstrates how nepheline is formed from the basic components.



Melilite and spinel are present in all samples from the slag cone but were not observed in samples from the product cone. This is a major mineralogical difference between both cones. As spinel, a magnesiochromite was selected for peak evaluation.

Table 2. Results of the semiquantitative WDXRF analysis of the product cone (sample no. 6 and 7) on pressed pallets with statistical error.

Sample	SiO ₂ [mass%]	SO ₃	Fe ₂ O ₃	CaO	Al ₂ O ₃	NiO	CuO	Na ₂ O	MgO	V ₂ O ₅
6	26.0 ± 0.25%	17.8 ± 0.22%	12.3 ± 0.09%	11.8 ± 0.21%	7.7 ± 0.43%	8.4 ± 0.11%	3.4 ± 0.14%	3.2 ± 1.02%	2.2 ± 0.81%	1.0 ± 0.73%
7	39.4 ± 0.20%	6.5 ± 0.37%	4.4 ± 0.16%	19.7 ± 0.17%	10.9 ± 0.34%	2.2 ± 0.18%	1.0 ± 0.25%	4.3 ± 0.81%	3.3 ± 0.62%	1.3 ± 0.68%

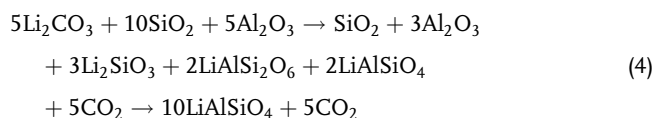
Table 3. Observed mineral phases in the slag samples from various positions as determined by qualitative analysis of powder diffraction patterns.

Phase	PDF. number	References	Chemical composition	Slag cone	Product cone
Clinopyroxene (augite)	00-078-1392	[57]	$\text{Al}_{0.3}\text{Ca}_{1.0}\text{Mg}_{0.7}[\text{Al}_{0.3}\text{Si}_{1.7}\text{O}_6]$	1b, 2, 3, 4, 5	6, 7
β -eucryptite	01-070-1574	[58]	$\text{LiAl}[\text{SiO}_4]$	1b, 2, 3	6, 7
Gehlenite (melilite)	01-079-2422	[59]	$\text{Ca}_2(\text{Mg}_{0.25}\text{Al}_{0.75})[\text{Si}_{1.25}\text{Al}_{0.75}\text{O}_7]$	1b, 2, 3, 4, 5	–
Lithium metasilicate	01-074-2145	[60]	$\text{Li}_2[\text{SiO}_3]$	4, 5	–
Nepheline	01-070-1260	[61]	$\text{K}_{0.25}\text{Na}_6[\text{Al}_{6.24}\text{Si}_{9.76}\text{O}_{32}]$	1b, 2, 3, 4, 5	6, 7
Pentlandite	01-078-0166	[62]	$\text{Fe}_{4.005}\text{Ni}_{4.995}\text{S}_8$	–	6, 7
Spinel (magnesiochromite)	01-078-1529	[63]	MgCr_2O_4	1b, 2, 3, 4, 5	–
Wollastonite	00-027-0088	–	$\text{Ca}[\text{SiO}_3]$	–	6, 7

Similar to the clinopyroxene, the exact composition of the spinel in the slag could deviate, as the spinel group can incorporate cations commonly found in the slag (e.g., Fe, Mn, Cr).^[36] Wollastonite can only be detected in the product cone as major calcium-bearing phase, which is, in the slag cone, mainly bound by the melilite. Clinopyroxene, melilite, spinel, and wollastonite are typical slag phases in nonferrous metal production.^[42] Pentlandite is only present in the product cone, which is consistent with the higher sulfur content detected in those samples.

The lithium is incorporated in two different phases: 1) β -eucryptite (LiAlSiO_4), which is present in most samples, and 2) lithium metasilicate (Li_2SiO_3), only detectable on the outside of the slag cone (sample no. 4 and 5). Both phases contain a higher lithium content than lithium-bearing minerals which are mined as lithium ore (Table 4).^[43] The chemical composition of the slag cone samples (sample no. 1–5) is very similar, which would imply that the cooling rate is the determining factor. According to Konar et al.^[44] the ratio of Li_2SiO_3 : LiAlSiO_4 determines whether lithium metasilicate or β -eucryptite forms first when cooling a melt. As lithium metasilicate can only be found in the outer layer of the slag cone (sample no. 4 and 5), which cools fastest, this proves that the lithium metasilicate forms first. In samples with slower cooling rates, in the center of the slag cone, only β -eucryptite was observed. Hence, it is assumed that lithium metasilicate is likely metastable in this system and reacts to β -eucryptite. This is further supported by Jochum & Reimanis^[45] describing the formation of lithium metasilicate

as metastable intermediate product in the reaction of Li_2CO_3 , SiO_2 , and Al_2O_3 to β -eucryptite at 1100 °C (Equation (4)).



4.3. Potential for Lithium Recoverability

In the slag, the lithium phases β -eucryptite and lithium metasilicate were observed. For a lithium recover process, lithium metasilicate is less relevant as it is proven to be thermodynamically metastable. To generate lithium metasilicate instead of β -eucryptite, the slag cone must be cooled down faster which would lead to smaller crystal sizes making a recovery increasingly difficult. Hence, the β -eucryptite should be the focus for a lithium recovery process.

To estimate the potential for lithium recovery, the theoretical amount of β -eucryptite was calculated based on the total amount of lithium in the slag. The calculation assumes that all lithium reacts to β -eucryptite and no other lithium-bearing phases are formed. It is further assumed that the β -eucryptite forms according to its stoichiometric formula and that no lithium is lost to other phases in the slag. The resulting slag would consist of 14.9% β -eucryptite. However, in such a complex slag, it is likely that some lithium is incorporated in other phases and that the β -eucryptite shows a nonstoichiometric composition, as β -eucryptite forms multiple solid solutions, which influence the composition of the final phase leading to a lower overall β -eucryptite content. In the present slag system, following solid solutions are most relevant: 1) β -eucryptite (LiAlSiO_4)—nepheline (NaAlSiO_4),^[46] 2) β -eucryptite (LiAlSiO_4)— β spodumene ($\text{LiAlSi}_2\text{O}_6$).^[47]

Using specific phases that collect and concentrate a target metal is an already described strategy, often referred to as EnAM.^[15,16] For lithium recovery, a phase like LiAlO_2 with a very high lithium content of up to 10.5 mass% is suggested.^[16,48] However, to form those phases, a very high amount of lithium must be present in the slag.^[48,49] A phase like LiAlO_2 or lithium metasilicate would be highly efficient for lithium recovery, but achieving an appropriate slag composition in an industrial setting may be challenging, as slag modifiers must be reduced to

Table 4. Calculated maximum stoichiometric lithium content of the lithium-bearing mineral phases in the slag and lithium ore minerals.

Phase	Stoichiometric composition ^[43,60]	Calculated maximum stoichiometric lithium content [mass%]
Lithium metasilicate	$\text{Li}_2[\text{SiO}_3]$	15.43
β -eucryptite	$\text{LiAl}[\text{SiO}_4]$	5.51
Spodumene	$\text{LiAl}[\text{SiO}_3]_2$	3.73
Petalite	$\text{LiAl}[\text{Si}_4\text{O}_{10}]$	2.27
Zinnwaldite	$\text{K}(\text{LiFe}^{2+}\text{Al})[(\text{AlSi}_3\text{O}_{10})(\text{F},\text{OH})_2]$	1.92 ^[43]
Lepidolite	$\text{K}(\text{LiAl}_2)[\text{Si}_3\text{O}_{10}](\text{OH},\text{F})_3$	2.74 ^[43]
Amblygonite	$\text{LiAl}[\text{PO}_4](\text{F},\text{OH})$	4.76
Jardarite	$\text{LiNaB}_3[\text{SiO}_7](\text{OH})$	3.16

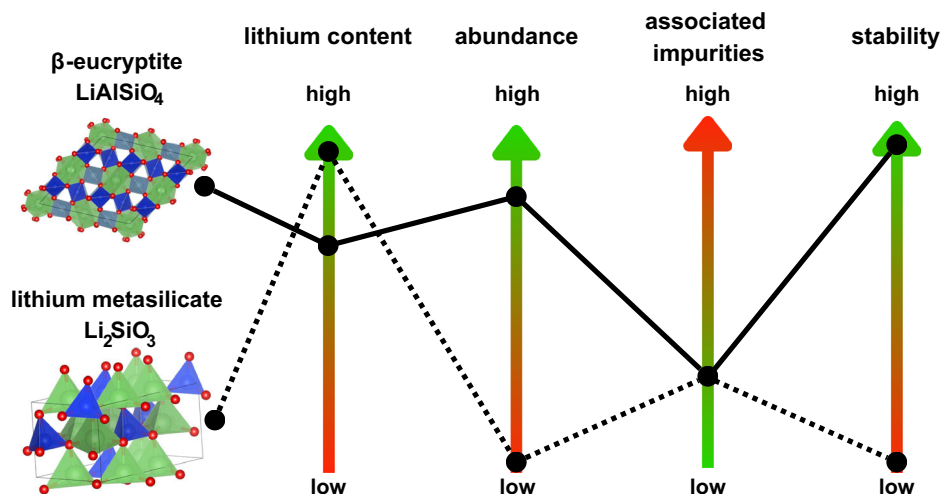


Figure 7. Advantages (green) and disadvantages (red) of the two detected lithium-bearing phases, β-eucryptite, and lithium metasilicate, for a lithium recovery process.

decrease the dilution of lithium in the slag. However, slag modifiers are important as they reduce the process temperatures by decreasing the degree of slag polymerization and thus achieve a workable viscosity at lower temperatures.^[50] The presented slag already contains a high-lithium-containing phase and comes from an economically feasible industrial process.

Additional to the high lithium content of β-eucryptite and a sufficient amount thereof, further parameters must be met to economically recover lithium from the slag. These are microstructure (crystal size, intergrowth) and present impurities.^[51,52] First, the crystal size and intergrowth patterns determine the degree of grinding.^[51] Grinding a material very fine is immensely energy intensive^[53] and leads to finer tailings, which are more difficult to handle.^[54] Currently, no complementary analyses have been carried out to quantify crystal size distribution or intergrowth patterns. Second, the pyrometallurgical processing aims to recover most of the Ni and Cu. The remaining Ni and Cu are impurities which can negatively impact a potential downstream hydrometallurgical extraction of lithium.^[55] The low content of Ni and Cu in the samples of the slag cone (sample no. 1–5) show that this is already possible.

Taking these aspects into account (Figure 7), the inner part of the slag cone (sample no. 2 and 3), exhibits the most promising composition for an economic recovery of lithium. If the microstructure (crystal size, intergrowth) of the β-eucryptite is sufficient, the lithium can be further concentrated, which allows for efficient hydrometallurgical extraction. The samples from the slag cap of the product cone (sample no. 6 and 7) still contain a lot of valuable Ni and Cu. To avoid issues in downstream hydrometallurgy, the precious metals should be recovered, e.g., by adding them back to the feedstock for the pyrometallurgy. The lithium from the outer parts of the slag cone (sample no. 4 and 5) is bound in lithium metasilicate, which is metastable, likely preventing the formation of larger crystals. The lithium can be recovered by bulk leaching. This would make a more complex hydrometallurgical treatment necessary and consume more process chemicals compared to only leaching a lithium enriched

phase. Both factors are challenging for an economic recovery of lithium.

5. Conclusion

Slag from an industrial lithium recycling process was analyzed by different chemical and mineralogical methods. A slag cone and the slag cap of a product cone from the same batch was analyzed. Significant mineralogical and chemical differences are observed between both cones. Chemically, the slag cap of the product cone contains less lithium and an increased amount of sulfur and associated metals compared to the slag cone. Mineralogically, other silicate minerals are found with wollastonite forming as the major Ca-bearing mineral instead of melilite. The increased sulfur content results in higher concentrations of metal sulfides, such as pentlandite. The high Ni and Cu content, which represents additional impurities for a downstream hydrometallurgical processing, makes the slag cap of the product cone undesirable for a lithium-focused recycling process. The slag cap can be best utilized by adding it back in the smelting process, to extract the Ni and Cu.

The slag cone shows little chemical variance, as shown by an overall low CV, and a constant lithium content of 0.82 mass%. Mineralogically, typical nonferrous slag minerals like clinopyroxene, spinel, melilite, and nepheline can be detected. The major mineralogical difference in the slag cone is the formation of lithium metasilicate on the outer parts of the slag cone (sample no. 4 and 5) while β-eucryptite forms in the main slag body (sample no. 1–3). For the recovery of lithium from the slag, the main slag body of the slag cone (sample no. 2 and 3) is the most promising. It contains low amounts of Ni and Cu and the stable of the β-eucryptite as lithium-bearing mineral. Furthermore, β-eucryptite from the inner part of the slag cone should have the largest crystal sizes. The lithium metasilicate contains more lithium, but is metastable, preventing the formation of larger crystals and is less abundant. Future work should focus on

quantifying the microstructure (crystal size, intergrowth) as well as verify the lithium content of all present phases.

Supporting Information

Supporting Information is available from the Wiley Online Library or from the author.

Acknowledgements

The authors want to express gratitude toward the research group Mineralogy and Geochemistry at the Martin-Luther-University Halle-Wittenberg and the colleagues from the Center of Resources and Recycling (CRR) at the Institute for Technologies and Economics of Lithium (ITEL). The authors want to thank Dr. Maximilian Korges from Potsdam University for his input and the valuable discussions about the manuscript and Dr. Maria Gaudig from ITEL and Martin-Luther-University Halle-Wittenberg for her aid with discussing some of the figures. The X-ray fluorescence spectrometer was funded by the Deutsche Forschungsgemeinschaft (DFG, German Research Foundation)—under grant no.: 658680, Martin Luther University Halle-Wittenberg (RM, BG, HP, CSS, GB). Furthermore, the authors want to thank the “Freundeskreis des Deutschen Lithiuminstitutes e.V.” for their funding. Finally, the authors want to express gratitude toward Nickelhütte Aue GmbH for their support and for providing the sample material.

Conflict of Interest

The authors declare no conflict of interest.

Author Contributions

Peter Cornelius Gantz: data curation (lead); formal analysis (lead); methodology (equal); visualization (lead); writing—original draft (lead). **Louisa Panjiyar:** data curation (supporting); writing—review & editing (supporting). **Andreas Neumann:** methodology (equal); writing—review & editing (equal). **Michael Neumann:** resources (lead); writing—review & editing (supporting). **Hans Roggendorf:** methodology (equal); supervision (equal); writing—review & editing (equal). **Ralf Wehrspohn:** conceptualization (lead); supervision (equal); validation (supporting); writing—review & editing (equal). **Stefan Stöber:** project administration (lead); supervision (equal); writing—review & editing (supporting). **Christiane Stephan-Scherb:** supervision (equal); visualization (supporting); writing—review & editing (lead).

Data Availability Statement

The data that support the findings of this study are available from the corresponding author upon reasonable request.

Keywords

β-eucryptites, lithium-ion batteries, lithiums, pyrometallurgies, recyclings, slags, smeltings

Received: October 14, 2024

Revised: November 22, 2024

Published online: December 15, 2024

- [1] G. Zubi, R. Dufo-López, M. Carvalho, G. Pasaoglu, *Renewable Sustainable Energy Rev.* **2018**, *89*, 292.
- [2] R. Somerville, P. Zhu, M. A. Rajaeifar, O. Heidrich, V. Goodship, E. Kendrick, *Resour. Conserv. Recycl.* **2021**, *165*, 105219.
- [3] V. Moreau, P. Dos Reis, F. Vuille, *Resources* **2019**, *8*, 29.
- [4] C. Hagelüken, D. Goldmann, *Miner. Econ.* **2022**, *35*, 539.
- [5] 2020/0353/COD, **2023**.
- [6] H. Zhou, Y. Yang, W. Li, J. McKechnie, S. Thiede, P. Wang, *One Earth* **2024**, *7*, P1288.
- [7] B. Swain, *Sep. Purif. Technol.* **2017**, *172*, 388.
- [8] L. Brückner, J. Frank, T. Elwert, *Metals* **2020**, *10*, 1107.
- [9] X. Hu, Y. Zhang, Z. Ding, T. Wang, H. Lian, Y. Sun, J. Wu, *Atmos. Environ.* **2012**, *57*, 146.
- [10] J. Li, G. Wang, Z. Xu, *Waste Manage.* **2016**, *52*, 221.
- [11] H. Li, H. Qiu, M. Ranneberg, H. Lucas, T. Graupner, B. Friedrich, B. Yagmurlu, D. Goldmann, J. Bremer, M. Fischlschweiger, *ACS Sustainable Resour. Manage.* **2024**, *1*, 1170.
- [12] S. Windisch-Kern, E. Gerold, T. Nigl, A. Jandric, M. Altendorfer, B. Rutrecht, S. Scherhauser, H. Raupenstrauch, R. Pomberger, H. Antrekowitsch, F. Part, *Waste Manage.* **2022**, *138*, 125.
- [13] S. Hampel, I. A. Alhafez, T. Schirmer, N. Merkert, S. Wunderlich, A. Schnickmann, H. Li, M. Fischlschweiger, U. E. A. Fittschen, *ACS Omega* **2024**, *9*, 24584.
- [14] F. Lourens, E. Suhr, A. Schnickmann, T. Schirmer, A. Ludwig, *Adv. Eng. Mater.* **2024**, *26*, 2302091.
- [15] C. Rachmawati, J. Weiss, H. I. Lucas, E. Löwer, T. Leißner, D. Ebert, R. Möckel, B. Friedrich, U. A. Peuker, *Minerals* **2024**, *14*, 130.
- [16] H. Qiu, H. Li, M. Fischlschweiger, M. Ranneberg, T. Graupner, H. Lucas, C. Stallmeister, B. Friedrich, B. Yagmurlu, D. Goldmann, *Miner. Eng.* **2024**, *217*, 108918.
- [17] B. Makuza, Q. Tian, X. Guo, K. Chattopadhyay, D. Yu, *J. Power Sources* **2021**, *491*, 229622.
- [18] J. Lee, K. W. Park, I. Sohn, S. Lee, *Int. J. Miner. Metall. Mater.* **2024**, *31*, 1554.
- [19] P. Liu, L. Xiao, Y. Tang, Y. Chen, L. Ye, Y. Zhu, *J. Therm. Anal. Calorim.* **2019**, *136*, 1323.
- [20] O. Kwon, I. Sohn, *Resour. Conserv. Recycl.* **2020**, *158*, 104809.
- [21] D. Cheret, S. Santen (Umicore), US 7169206 B2, **2005**.
- [22] M. Quix, D. van Horebeek, T. Suetens (Umicore), AU 2017206924 B2, **2017**.
- [23] Y. Jie, S. Yang, Y. Li, D. Zhao, Y. Lai, Y. Chen, *Minerals* **2020**, *10*, 949.
- [24] G. Lombardo, B. Ebin, M. R. St. J. Foreman, B.-M. Steenari, M. Petranikova, *J. Hazard. Mater.* **2020**, *393*, 122372.
- [25] G. Lombardo, B. Ebin, M. R. St. J. Foreman, B.-M. Steenari, M. Petranikova, *ACS Sustainable Chem. Eng.* **2019**, *7*, 13668.
- [26] S. Babanejad, H. Ahmed, C. Andersson, C. Samuelsson, A. Lennartsson, B. Hall, L. Arnerlöf, *J. Sustainable Metall.* **2022**, *8*, 566.
- [27] L. Sun, K. Qiu, *J. Hazard. Mater.* **2011**, *194*, 378.
- [28] N. Zachmann, M. Petranikova, B. Ebin, *J. Ind. Eng. Chem.* **2023**, *118*, 351.
- [29] DIN EN ISO, 11885, **2009**.
- [30] DIN, 51085, **2015**.
- [31] A. B. Blank, L. P. Eksperiandova, *X-ray Spectrom.* **1998**, *27*, 147.
- [32] S. Amiri, S. Zwanig, *J. Chemom.* **2011**, *25*, 295.
- [33] M. Watanabe, H. Inoue, Y. Yamada, M. Feeney, L. Oelofse, Y. Kataoka, *Powder Diffr.* **2013**, *28*, 132.
- [34] J. G. Dunn, *Thermochim. Acta* **1997**, *300*, 127.
- [35] C. Kleeberg, *Mater. Sci. Technol.* **2022**, *38*, 607.
- [36] F. Bosi, C. Biagioni, M. Pasero, *Eur. J. Mineral.* **2019**, *31*, 1.
- [37] T. Degen, M. Sadki, E. Bron, U. König, G. Nénert, *Powder Diffr.* **2014**, *29*, 13.
- [38] G. S. Pawley, *J. Appl. Crystallogr.* **1981**, *12*, 357.
- [39] A. A. Coelho (Bruker AXS), TOPAS V.6.0, **2018**.

- [40] M. Cameron, J. J. Papike, *Am. Min.* **1981**, 66, 1.
- [41] X. Meng, Y. Li, H. Wang, Y. Yang, A. Mclean, *J. Hazard. Mater.* **2020**, 399, 122845.
- [42] N. M. Piatak, M. B. Parsons, R. R. Seal, *J. Appl. Geochem.* **2015**, 57, 236.
- [43] B. Tadesse, F. Makuei, B. Albijanic, L. Dyer, *Miner. Eng.* **2019**, 131, 170.
- [44] B. Konar, D.-G. Kim, I.-H. Jung, *J. Eur. Ceram. Soc.* **2018**, 38, 3881.
- [45] T. Jochum, I. Reimanis, *J. Am. Ceram. Soc.* **2010**, 93, 1591.
- [46] J. Marcial, J. Kabel, M. Saleh, N. Washton, Y. Shaharyar, A. Goel, J. S. McCloy, *J. Am. Ceram. Soc.* **2018**, 101, 2840.
- [47] R. Roy, D. M. Roy, E. F. Osborn, *J. Am. Ceram. Soc.* **1950**, 33, 152.
- [48] H. Li, H. Qiu, M. Ranneberg, H. Lucas, T. Graupner, B. Friedrich, B. Yagmurlu, D. Goldmann, J. Bremer, M. Fischlschweiger, *ACS Sustainable Resour. Manage.* **2024**, 1, 1170.
- [49] H. Li, H. Qiu, T. Schirmer, D. Goldmann, M. Fischlschweiger, *ACS EST Eng.* **2022**, 2, 1883.
- [50] K. Mills, M. Guo, *ISIJ Int.* **2014**, 54, 2000.
- [51] L. Pérez-Barnuevo, E. Pirard, R. Castroviejo, *Miner. Eng.* **2013**, 52, 136.
- [52] J. P. H. Perez, K. Folens, K. Leus, F. Vanhaecke, P. van der Voort, G. Du Laing, *Resour. Conserv. Recycl.* **2019**, 142, 177.
- [53] J. A. Curry, M. J. Ismay, G. J. Jameson, *Miner. Eng.* **2014**, 56, 70.
- [54] D. Q. Deng, L. Liu, Z. L. Yao, K. I.-I. L. Song, D. Z. Lao, *J. Environ. Manage.* **2017**, 196, 100.
- [55] C. Peng, K. Lahtinen, E. Medina, P. Kauranen, M. Karppinen, T. Kallio, B. P. Wilson, M. Lundström, *J. Power Sources* **2020**, 450, 227630.
- [56] J. Mutterer, E. Zinck, *J. Microsc.* **2013**, 252, 89.
- [57] Y. P. Ahn, B. H. Kim, N. Ishizowa, *J. Korean Ceram. Soc.* **1986**, 23, 25.
- [58] V. Tscherry, H. Schulz, F. Laves, *Z. Kristallogr. – Cryst. Mater.* **1972**, 135, 175.
- [59] I. Swainson, M. Dove, W. Schmahl, A. Putnis, *Phys. Chem. Miner.* **1992**, 19, 3.
- [60] B. A. Maksimov, Yu. A. Kharitonov, V. V. Ilyukhin, N. V. Belov, *Dokl. Akad. Nauk SSSR* **1968**, 178, 1309.
- [61] W. A. Dollase, W. M. Thomas, *Contr. Miner. Petrol.* **1978**, 66, 311.
- [62] V. Rajamani, C. T. Prewitt, *Am. Min.* **1975**, 60, 1.
- [63] H. C. St. O'Neill, W. A. Dollase, *Phys. Chem. Miner.* **1994**, 20, 541.